Electrical Properties of Supported Lipid Bilayer Membranes

Gerald Wiegand,[†] Noah Arribas-Layton,[†] Heiko Hillebrandt,[‡] Erich Sackmann,[‡] and Peter Wagner*,[†]

Zyomyx, Inc., 26101 Research Road, Hayward, California 94545, and Physik Department, Biophysics Group, Technische Universität München, James-Franck-Strasse, D-85748 Garching, Germany

Received: November 29, 2001; In Final Form: January 24, 2002

This paper describes a study of the electrical properties of supported lipid bilayer membranes on semiconductor and gold surfaces. The study is aimed to foster the understanding of supported membrane systems and to allow the rational design of biosensor assays for ion channel analysis. Impedance spectroscopy was applied for the electrical characterization of the supported membrane systems. A novel equivalent circuit model is introduced for the data evaluation, which accounts for the deviation of the impedance response of supported membranes from that of an ideal RC element. As a result of the improved accordance of model and data, the resistance and the capacity of supported membranes can be determined more accurately and independently from each other. Experimental results describe the phenomenology of the electrical properties of supported bilayers regarding variations in preparation, composition, and environmental conditions. We discuss the findings in terms of membrane−substrate interactions and models of membrane permeability. The important role of the electrostatics between the lipid bilayer and the solid substrate for the formation of an electrically dense supported membrane is identified. Bilayer permeability models explain the correlation between the structure of the lipid bilayer and its insulating properties. These models are also in accordance with the observed dependence of the electrical resistance of the lipid bilayer on the temperature and the ion concentration of the electrolyte.

Introduction

Solid supported lipid bilayer membranes (SSM) were studied over recent years as a promising assay format for on-chip characterization of membrane proteins.[1−3] The understanding of the formation process of SSMs and the dependence of their properties on environmental and compositional parameters is an important prerequisite for the reliable preparation of functional assays. Ultimately, it shall enable the rational design of SSM applications on top of sophisticated micromachined chip devices accessible for accurate and highly sensitive detection technology.

Ion channels represent one class of target proteins for SSM assays.[3−6] To study ion channels in SSMs, an electrically dense lipid bilayer matrix surrounding the embedded proteins has to be provided. Many SSM systems described in the literature do not qualify as electrically dense membranes, because the reported defect densities minimize the insulation properties of the lipid bilayers. This is particularly valid for systems with a highly hydrated polymeric separation layer between membrane and substrate.[7−9] The standard for the analysis of ion channels is set by the black lipid membrane technique[10] (BLM) and the patch-clamp (PC) technique.[11] Both techniques work with highly insulating lipid bilayers generated either by a bilayer suspended over an aperture or by a membrane patch at the end of a micropipet. In comparison, typical values of the electrical resistance of SSMs (10^{-3} to 1 MΩ cm^2)[4,6,12] are still lower than the ones obtained, e.g., with the BLM technique (> 10 MΩ cm^2).[10]

In this paper, we describe the electrical characterization of SSMs (Figure 1) by impedance spectroscopy (IS). IS provides comprehensive information about the dominant electrical process of the system under investigation.[13] Impedance spectra are evaluated by fitting the impedance response of an equivalent circuit model to the measured data. A novel equivalent circuit model for SSMs is derived accounting for the distributed impedance response of lipid bilayers.

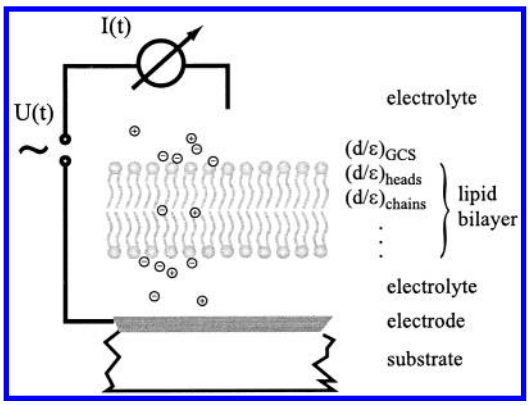

Figure 1. Schematic view of a supported membrane (SSM) on an electrode substrate. The lipid bilayer exhibits a stratified substructure composed of the Gouy−Chapman−Stern (GCS) layer, the lipid headgroup region, and the region of the alkyl-chains for both monolayers. All layers exhibit different electrical thicknesses, d/ϵ. There is an electrolyte film of about 1−1.5 nm thickness between the lipid bilayer and the solid support.

Indium−tin oxide and doped silicon were employed as semiconductor electrode materials. In addition, thin films of gold functionalized with self-assembled monolayers (SAM) were utilized as electrodes. The formation of electrically dense SSMs was investigated with respect to the pH of the electrolyte and the concentration of charged lipids and cholesterol contained in the bilayers. The dependence of the membrane properties on the temperature and the ionic concentration of the electrolyte

* Fax: +1 510 266 7792. Telephone: +1 510 266 7500. E-mail: pwagner@zyomyx.com.
[†] Zyomyx, Inc.
[‡] Technische Universität München.

10.1021/jp014337e CCC: $22.00
Published on Web 03/28/2002

was monitored. Other aspects such as the method of bilayer formation and the size of the electrodes are correlated to the experimental results. Membrane−substrate interactions and membrane permeability models[14,15] are considered for the interpretation of the data and the comparison of the SSMs with unbound membranes.

Materials and Methods

Materials. Cholesterol and the lipids 1,2-dimyristoyl-sn-glycero-3-phosphocholine (DMPC), 1,2-dioleoyl-sn-glycero-3-phosphocholine (DOPC), 1,2-dioleoyl-3-trimethylammonium propane (DOTAP), 1,2-dimyristoyl-3-trimethylammonium propane (DMTAP) were purchased from Avanti Polar Lipids. All other chemicals such as solvents and buffer substances were purchased from Sigma Aldrich and used as delivered without further purification. The water used was ion-exchanged and Millipore-filtered (Millipore Milli-Q-System, Molsheim, France, $R > 18$ MΩ cm^{-1}, pH 5.5). Buffer solutions were degassed thoroughly. NaCl was added to the buffer solution for experiments with varying ion concentration. The osmolality of the buffer solutions was determined by means of an osmometer (Advanced Instruments/Norwood).

Electrodes and Measuring Cell. Three different electrode materials were utilized: (1) indium−tin-oxide (ITO), (2) doped silicon, and (3) gold.

(1) ITO electrodes were fabricated by a standard lithographical procedure from glass slides coated with an ITO film of 100 nm thickness (Baltracon 247, Balzers AG, Liechtenstein) with detection areas of either 0.007 ± 0.0015 cm^2 or 0.09 ± 0.01 cm^2 per ITO electrode. Two identical ITO electrodes were connected as working and counter electrodes in an IS experiment.

(2) Chips of p-type silicon (5−10 Ω cm) were used for the silicon electrodes. A film of 5 nm titanium and 100 nm gold was evaporated on the backside of the chip to allow ohmic contact to the measurement circuitry. The surface of the detection site is covered by native oxide. Again, two different layouts led to detection areas of either 0.17 ± 0.02 cm^2 or 0.04 ± 0.005 cm^2. Platinized platinum wires were used as counter electrodes with the silicon working electrodes. Both ITO and silicon substrates were cleaned according to the following procedure: rinsing in ethanol for 2 min; ultrasonic treatment in acetone for 5 min with subsequent drying; ultrasonic treatment in a solution of 15% (v/v) ammonium hydroxide (30%), 15% hydrogen peroxide (30%), and 70% water for 5 min; heating of the same solution to 60 °C for 30 min; and intensive rinsing in water.

(3) For the gold electrodes, layers of 5 nm titanium and 100 nm gold were evaporated subsequently onto the polished side of silicon chips. The gold working electrodes had an area of 0.04 ± 0.005 cm^2 and were measured against platinized platinum wire counter electrodes.

The substrates were mounted into a measuring cell. The measuring cell formed a liquid chamber of 0.25 mL volume by sealing the top plate of the cell to the substrate. The temperature of the measuring cell was varied by water flux through the bottom plate of the measuring cell. One to four identical but separate measuring cells were analyzed in parallel.

Self-Assembled Monolayer (SAM) Preparation. Prior to membrane deposition, the surface of gold electrodes needs to be functionalized with a SAM. The gold electrodes were functionalized by SAMs of mercaptoundecanoic acid (MUA) in order to render the surface hydrophilic. MUA was dissolved in ethanol at a 1 mM concentration. The substrates were immersed in the ethanol/MUA solution immediately after the deposition of the gold films and were incubated for at least 12 h. The substrates were rinsed thoroughly with pure ethanol and dried by nitrogen flow prior to being mounted in the measuring cell.

Preparation of Supported Membranes. Two different techniques for the preparation of electrically dense supported lipid membranes were applied: the vesicle fusion method and the solvent exchange method.

For the vesicle fusion, suspensions of lipid vesicles in buffer solution were prepared according to the following procedure. Lipid from chloroform stock solutions was desiccated and stored under vacuum for at least 2 h. For mixtures, appropriate amounts of stock solution of the respective compounds were mixed before desiccation. Throughout this paper, molar ratios are provided for lipid mixtures. Buffer solution was added to the dried lipid (1 mg of lipid per ml buffer solution). At least 2 h was allowed for hydration. Five cycles of freezing (liquid nitrogen) and thawing (water bath at 50 °C) were applied to the lipid suspensions. If not used instantaneously, the vesicle suspensions were stored after the last freezing step at −20 C for up to 4 weeks. Immediately before injection into the measuring cell, the vesicle suspension was sonicated for 10 min.

For the solvent exchange method, stock solutions of the different pure lipids or lipid mixtures were prepared by adding 2-propanol to the dried lipid instead of buffer solution. The lipid concentration was 10 mg/mL. 2-Propanol solution containing the dissolved lipid mixture was injected into the measuring cell. Subsequently, the cell was rinsed slowly with aqueous buffer solution. Since water and 2-propanol are miscible, the addition of the buffer has to reach a critical concentration until the lipid molecules aggregate. A supported bilayer is formed in the vicinity of the substrate, while vesicles are formed in the bulk. The rinsing of the cell was interrupted before all vesicles were removed from the cell to allow further healing of the membrane.

Impedance Spectroscopy (IS). Impedance spectroscopy is an AC technique. The complex electrical impedance $Z(\omega)$ is determined by the ratio between the voltage signal $U(\omega)$ applied to the sample and the measured current response $I(\omega)$ of the sample as a function of the frequency,

$$Z(\omega) = \frac{U(\omega)}{I(\omega)} = Z_0(\omega) \cdot e^{i\varphi(\omega)} \tag{1}$$

The polar coordinates of $Z(\omega)$, the absolute value of the impedance $Z_0(\omega)$, and the phase $\varphi(\omega)$ are used for data representation. Impedance measurements were performed within the frequency range of 10^{-1} to 10^5 Hz with five measurement points per frequency decade. The amplitude of the applied voltage signal was 50 mV. Commercially available impedance analyzers were utilized for data acquisition (i: SI 1260, Schlumberger Technologies; ii: PGSTAT30 & FRA module, EcoChemie). Impedance data were analyzed by a self-written procedure using the software package Igor Pro (Wavemetrics).

Model for the Impedance Behavior of Supported Membranes. To evaluate the measured impedance spectra, a model providing a mathematical expression for the electrical response of the system under investigation is required. The electrical response of most bulk materials and interfaces is either ohmic or capacitive. Therefore circuit models can be assembled from resistors and capacitors representing the electrically dominant components of a system. These circuit models are called equivalent circuits.[13] The standard equivalent circuit for SSM systems is shown in Figure 2a. It comprises a series resistor for the electrolyte resistance R_{EL} and two RC elements, one

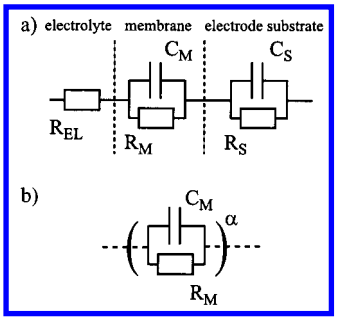

Figure 2. Equivalent circuits models for SSM structures. (a) Simple equivalent circuit comprising the electrolyte resistance R_{EL} in series to a parallel connection of the membrane resistance R_M and the membrane capacity C_M and the $(RC)_S$-element representing the electrode substrate. Depending on the electrode material, R_S and C_S have different origins. (b) RC-element with distributed time constants expressed by the parameter α substituting the membrane part of the circuit in part a.

representing the membrane by the parallel connection of the membrane capacity C_M and the membrane resistance R_M and the other representing interfacial properties of the supporting electrode by the parallel connection of the capacity C_S and the resistance R_S. Depending on the electrode material, the origin of C_S and R_S differs. The expression for the impedance of the circuit is given by

$$Z(\omega) = Z_{EL}(\omega) + Z_M(\omega) + Z_S(\omega) = R_{EL} + \left(\frac{1}{R_M} + i\omega C_M\right)^{-1} + \left(\frac{1}{R_S} + i\omega C_S\right)^{-1} \quad (2)$$

Fitting the impedance response of this simple equivalent circuit to measured data of a SSM system (Figure 3) reveals limited accordance between model and data. The residuals of the fit plotted in Figure 4indicate significant deviations. The main drawbacks of the limited accordance of this simple model and the data are (i) the reduced accuracy of the values determined and (ii) the transfer of variations of one parameter into variations of the other parameters. The latter is of importance for any systematic study of membrane properties, since changes of the membrane resistance lead to changes of the membrane capacity and vice versa without physical causality. Therefore, an improved model is required to eliminate artifacts introduced by the equivalent circuit analysis.

The simple model circuit is based on the assumption of a stratified structure of homogeneous layers and distinct interfaces. This assumption is appropriate for the bulk electrolyte and the electrode substrate, but it oversimplifies the SSM. Lateral heterogeneities, such as defects or domains,[16−18] and structural heterogeneities[16] perpendicular to the plane of the lipid bilayer have to be distinguished. An equivalent circuit containing a parallel connection of multiple RC elements for the SSM instead of one RC element can model lateral heterogeneities. By consideration of Kirchhoff's laws for the combination of circuit elements, the parallel connection of RC elements could be reduced again to a single RC element with an averaged value for the resistance and the capacitance but no difference in the frequency dispersion. Therefore, such a parallel connection of RC elements cannot account for the observed deviations. In the perpendicular direction, along the axis of the lipid molecules, several molecular regions with different electrostatic properties do exist.[16] Each leaflet of the bilayer is composed of three layers (see Figure 1), the Gouy−Chapman−Stern (GCS) layer, the layer of the lipid headgroups, and the layer of the alkyl chains of the lipids. All of these layers exhibit different dielectric thickness, d_i/ϵ_i, and thus, capacities. Presumably, the layers also

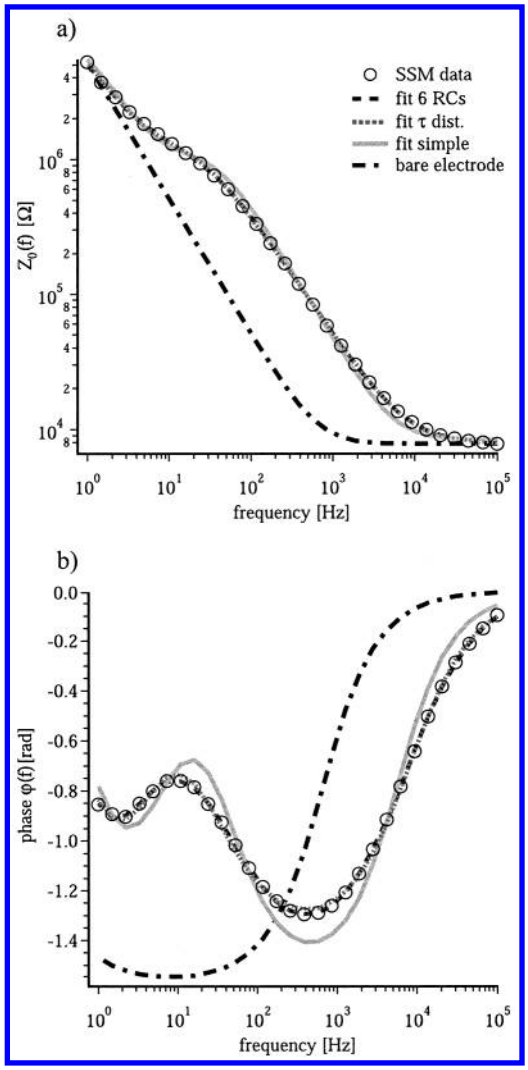

Figure 3. Impedance data (○) and corresponding fits for a supported lipid bilayer on ITO electrodes (0.007 cm^2). The impedance of a bare electrode is given (- • -) for comparison. For data fitting, the simple model (—), the model of distributed time constants τ (···), and the model of a series connection of six RC elements (- - -) were applied. The two latter models are in good agreement with the data. The values of R_M and C_M obtained by the different models are provided in Table 1. R_{EL} = 7.8 kΩ, C_S = 4.8 μF/cm^2, and R_S = 61 kΩ cm^2 were obtained by using the model of distributed time constants.

exhibit different ion permeabilities, and the broken symmetry of the bilayer due to the adjacent substrate may lead to different properties for the two leaflets. Due to the molecular dimensions, the interfaces between the individual layers of the stratified film are not sharp but vary continuously. To account for this heterogeneity, the number of RC elements in series has been increased in the following approach. By fitting such a model to the impedance data in Figure 3, the residuals decreased with the addition of more RC elements up to a total of six (Figure 4). More than six RC elements did not further reduce the residuals significantly.

The large number of independent variables associated with such a model does not allow an unambiguous analysis of the membrane under varying condition. Therefore, we adopt a model that was derived by Cole and Cole,[19] which these authors used to account for the distributed dielectric relaxation of dipolar liquids. The product of the resistance R and the capacity C can be expressed in terms of a characteristic time constant τ by

$$\tau = R \cdot C \quad (3)$$

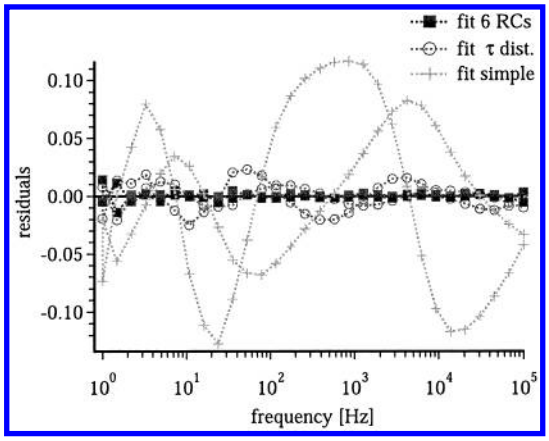

Figure 4. Plot of the residuals obtained by fitting the different models to the data in Figure 3. The residuals decrease from the simple model (+) to the model of distributed time constants τ (○) and the model of the series connection of six RC elements (■), which indicates the increasing agreement of model and data. The curves for both polar coordinates $Z_0(\omega)$ and $\varphi(\omega)$ are superimposed.

Note that in the case of a parallel connection of R and C, τ is not considered as a relaxation time but represents a characteristic time constant of the connection similar to that of a filter. The impedance of an RC element can now be written as $Z_{RC} = R/(1 + i\omega\tau)$. Analogously to Cole and Cole, we introduce the exponent α representing a distribution of time constants in order to replace the linear array of six RC elements of the previous approach. The expression for the impedance of the SSM follows as

$$Z_{M^a} = \frac{R_M}{1 + (i\omega\tau)^\alpha} \tag{4}$$

The value of $\alpha = 1$ corresponds to the situation of a single ideal RC element. Fuoss and Kirkwood derived analytically the distribution of time constants that is associated with the exponent α. This distribution is given by[20]

$$F_\alpha(s)\,ds = \frac{1}{2\pi} \cdot \frac{\sin[(1-\alpha)\pi]}{\cosh[\alpha(s - s_0)] - \cos[(1-\alpha)\pi]} \cdot ds \tag{5}$$

with

$$s = \log_{10}\tau \tag{6}$$

In this model, τ_0 is the center or the first moment of the distribution of time constants characterizing the SSM, and the values of the membrane resistance R_M and the membrane capacity C_M can be derived according to eqs 3 and 4.

Inserting eq 4 in to eq 2 provides the expression for the impedance $\mathbf{Z}(\boldsymbol{\omega})$ of the entire system. The fit of the model to the data in Figure 3 indicates good agreement. The residuals given in Figure 4 are slightly larger than with the six RC elements but substantially smaller than with the single RC element of the simple model. The values obtained by fitting the three different models to the data in Figure 3 are summarized in Table 1. In Figure 5, the distribution of time constants associated with α (eq 5), is shown together with a distribution $F_{RC}(s)$ obtained from the model of six RC elements. A Gauss distribution[20] is provided for comparison. $F_{RC}(s)$ was calculated according to the following equations

$$\int_{-\infty}^{\infty} F_{RC}(s)\,ds = \sum_{i=1}^{N} F_i(s) \cdot \Delta s_i = 1 \tag{7}$$

with $N = 6$ as the total number of available time constants τ_i.

$$F_i(s) = \frac{1}{N\Delta s_i} \tag{8}$$

Δs_i was defined as

$$\Delta s_i = \frac{|s_{i+1} - s_{i-1}|}{2} \tag{9}$$

s was restricted to the experimentally accessible range of −6 to −1.

Distributions similar to $F_\alpha(s)$ are also found for other transport phenomena. In disordered materials, the transport of charge carriers do not exhibit random diffusion, which means the loss of translational invariance. It is considered as a hopping and trapping process with a non-Gaussian distribution of resting times and jump distances, respectively. In the Fourier space, these distributions often exhibit power laws and are known as Levy distributions.[13,21] The power law behavior is a consequence of the correlation between the probability distribution of jump events and the distribution of energy levels, e.g., as in amorphous semiconductors.[22]

Due to the improved accordance obtained with just one additional independent variable, the model with distributed time constants was utilized for the data analysis of the experiments presented in this paper. The accuracy of the values of the membrane characterizing quantities R_M, C_M, and α obtained by the data-fitting procedures was in general <5% relative error. Close to the lower detection limit of the measurements the relative error increased, but never exceeded 15%. Depending on the size of the utilized working electrode, the lower detection limit ranged from $R_M = 20-500\ \Omega\ cm^2$.

Phenomenology of the Electrical Properties of Supported Lipid Bilayers. Experiments were performed to determine the dependence of the electrical properties of SSMs on compositional, preparative, and environmental parameters. Once a SSM is formed, the membrane capacity C_M does not vary significantly, since the bilayer structure determines its value. On the other hand, the membrane resistance, R_M, may alter over several orders of magnitudes in response to the mentioned variations and therefore indicates whether a membrane is electrically dense or not. Area-normalized values of both R_M and C_M are provided.

Solution pH. In Figure 6a, the membrane resistance R_M is shown as a function of the solution pH during SSM formation as obtained for 1:1 DOTAP/cholesterol membranes on silicon electrodes. Two series of four experiments were conducted, the first with 10 mM Hepes buffer titrated with NaOH to pH values in the range of 7.4−8.0 and the second with 10 mM Tris buffer titrated with HCl to pH values in the range of 8.0−8.6. The data are corrected for the different salt concentrations due to the titration (see Ion Concentration subsection). In both series, R_M increases for about an order of magnitude from the lowest to the highest pH. In addition, there is a significant difference between the membranes formed in Hepes buffer and the ones formed in Tris. The latter exhibits substantially better insulating properties, though it is not possible to discriminate from the data whether the buffer substances or the ions used for titration do account for it. The respective values of C_M were in the range 0.74−0.90 $\mu F/cm^2$ for all membranes that exhibited membrane resistance values >1 $k\Omega\ cm^2$. Close to the detection limit ($R_M \approx 0.3\ k\Omega\ cm^2$ in these experiments), the values obtained for C_M increase as a consequence of the lack of significance of the data.

TABLE 1: Summary of the Variables of the Supported Membrane Evaluated from the Impedance Data Shown in Figure 3 According to the Presented Models

			model of six RC elements					
	simple model	model of τ^{α} ($\alpha = 0.888$)	$i = 1$	$i = 2$	$i = 3$	$i = 4$	$i = 5$	$i = 6$
$R_{M,i}$ (kΩ cm^2)	4.28	5.40	0.0039	0.016	0.059	0.80	2.8	2.2
$C_{M,i}$ (μF/cm^2)	0.863	1.18	1.8	2.9	5.5	2.3	1.9	9.0
τi (ms)	(3.7)	6.4	0.0069	0.047	0.33	1.9	5.4	19

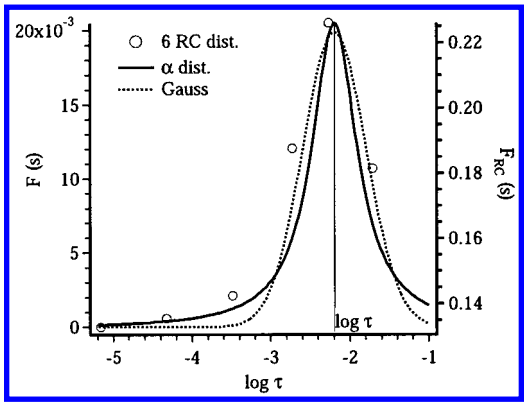

Figure 5. Distribution of time constants $F(s)$ for $\alpha = 0.888$ according to eq 5 (—) and $F_{RC}(s)$ for the model of six RC elements (○; eqs 7−9). The corresponding Gauss distribution[20] (•••) is shown for comparison.

The same series were applied to Au/MUA substrates (data not shown); however, no membranes were formed for any of the Hepes buffers. By using the Tris buffers, the tendency of increasing values of R_M with increasing pH was reproduced, but it was less pronounced and the absolute values were lower.

Figure 6b depicts the changes of R_M measured for a preformed SSM that was exposed subsequently to buffer solutions of decreasing pH. The plot provides the actual time course of the experiment, and the different pH levels of the buffer solutions are indicated (again 10 mM Tris and 10 mM Hepes). The variation of the Tris buffer from pH 8.6 to 8.0 in 0.2 increments did not affect the membrane significantly. The initial increase can be attributed to the fusion of vesicles that were not washed off the membrane surface by the preceding rinsing step. By switching to Hepes buffer, R_M started to decrease. All further pH reductions led to the destabilization of the membrane. C_M remained constant throughout the experiment at 0.76 ± 0.04 μF/cm^2.

Concentration of Charged Lipids. The values of R_M obtained for mixed SSMs formed by the neutral lipid DOPC and the cationic lipid DOTAP are shown in Figure 7 as a function of the molar concentration of DOTAP in the bilayers. The experiments were performed on both silicon substrates (Figure 7a) and Au/MUA substrates (Figure 7b) in 10 mM Tris buffer at pH 8.6. The variation of the concentration of charged lipid has a substantial impact on the quality of the membranes formed. On the oxide surface of the silicon substrates, a distinct maximum of R_M was detected at 10% DOTAP, which was reproduced in a second run of experiments with DOTAP concentrations from 0%−50%. On Au/MUA surfaces, the maximum is shifted toward 30% and is less pronounced, and the absolute values of R_M are lower. No detectable membrane was formed on Au/MUA in the absence of DOTAP, and two SSMs with instabilities at a late stage of the experiment are indicated by hollow symbols in Figure 7b. The membrane capacities of the different membranes were constant after the initial membrane formation phase and ranged from 0.86 to 1.12 μF/cm^2.

Concentration of Cholesterol. Cholesterol is present in many biological membranes at various concentration levels. The influence of cholesterol on the electrical properties of SSMs was studied by mixed DOTAP/cholesterol bilayers on silicon substrates in 10 mM Tris buffer at pH 8.6 (Figure 8). Four different DOTAP/cholesterol ratios were probed on electrodes of two different sizes. A significant increase of R_M with increasing cholesterol concentration was observed. For DOTAP/cholesterol mixtures, the variation of the cholesterol content implies the inverse variation of content of charged lipid in the bilayer; hence, the results represent the superposition of both effects. Despite this, the observed dependency can be attributed to the influence of cholesterol, because the absolute values of R_M are higher and the increase is substantially larger than in the comparable regime of the experiments with DOPC/DOTAP

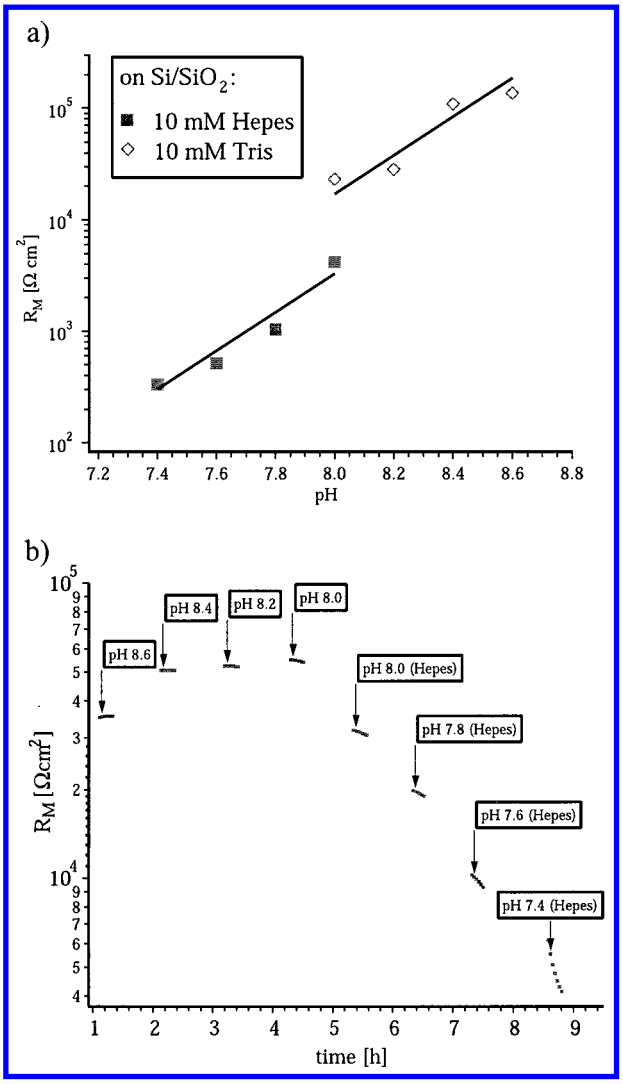

Figure 6. (a) Dependence of membrane resistance R_M on the solution pH during SSM formation. 1:1 DOTAP/cholesterol bilayers on Si/SiO$_2$ substrates were studied. pH 7.4−8.0: 10 mM Hepes buffer titrated with NaOH. pH 8.0−8.6: 10 mM Tris buffer titrated with HCl. Linear fits of the four data points measured with either Hepes or Tris buffer are provided. (b) Time course of the membrane resistance of a single bilayer exposed to a series of buffer solutions with decreasing pH values.

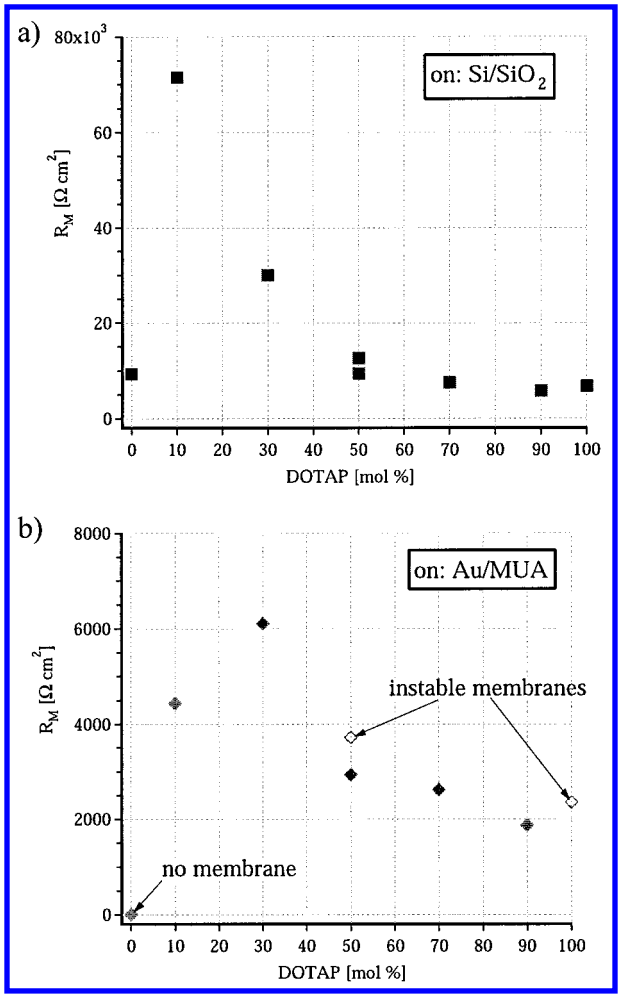

Figure 7. Dependence of the membrane resistance R_M on the concentration of cationic lipid contained in the SSM. Mixed DOTAP/DOPC bilayers were probed on (a) Si/SiO_2 and (b) Au/MUA substrates in 10 mM Tris buffer at pH 8.6.

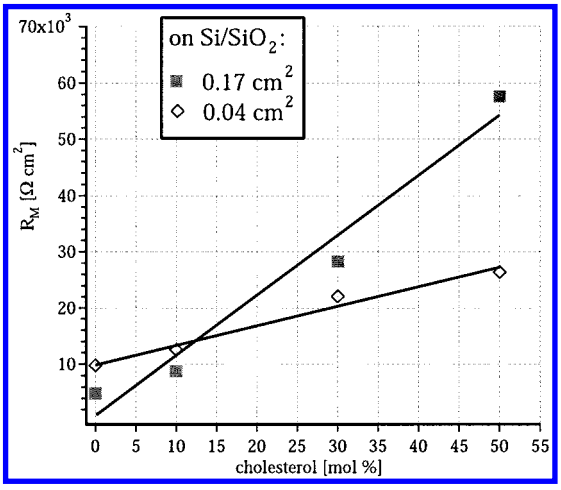

Figure 8. Dependence of the membrane resistance R_M on the concentration of cholesterol in the SSM. Mixed DOTAP/cholesterol bilayers were probed on Si/SiO_2 substrates in 10 mM Tris buffer at pH 8.6. A series of experiments was performed on electrodes with both 0.17 cm^2 and 0.04 cm^2 detection area. Linear fits of the four data points of each series are provided.

mixtures (50%−100% DOTAP in Figure 7a). The respective values of C_M were in the range 0.75−0.83 $\mu F/cm^2$.

Electrode Size. According to the datasets depicted in Figure 8, the size of the electrodes does apparently affect the area-normalized membrane resistance of SSMs. Experiments with SSMs on ITO substrates of two different sizes yielded in general higher values of R_M on electrodes with larger detection areas than on electrodes with smaller detection areas. This provides evidence that size and geometry of the electrodes cannot be neglected in the interpretation of electrical data of SSMs. The interfacial properties in the homogeneous areas of the electrode are invariant to scaling, but the border of the electrode represents a discontinuity of the stratified structure of SSM systems. Therefore, the ratio of the area to the circumference may provide a measure for the dependence of R_M on geometrical parameters, which has to be proven by further experiments.

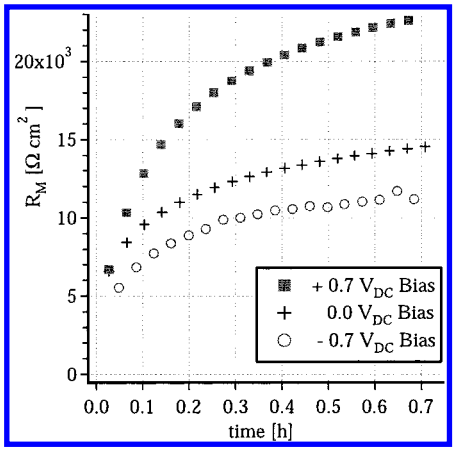

Figure 9. Evolution of the membrane resistance R_M during the SSM formation at different DC bias potentials. The bias potentials were applied between the silicon working electrode and a platinized platinum wire as counter electrode. 1:1 DOTAP/cholesterol membranes were formed in 10 mM Tris buffer at pH 8.6.

Bias Potential during Membrane Formation. Figure 9 shows the time courses of R_M obtained during the SSM formation with different dc bias voltages applied between the silicon working electrode and the platinum wire counter electrode. 1:1 DOTAP/cholesterol SSMs were deposited in 10 mM Tris at pH 8.6. Positive bias voltages leading to more negative surface potentials at the silicon oxide−electrolyte interface result in higher values of R_M and faster kinetics of SSM formation in comparison to 0 V bias voltage. The opposite, lower values of R_M and slower kinetics were observed for negative bias voltages. SSM formation did occur over the entire bias voltage range of +0.7 to −0.7 V that was analyzed.

Method of Membrane Formation. On ITO electrodes, two different methods were employed for SSM formation: the vesicle fusion and the solvent exchange method. The best result for a 1:1 DOTAP/cholesterol bilayer formed by vesicle fusion in 10 mM Hepes at pH 7.5 yielded a membrane resistance of $R_M = 22\ k\Omega\ cm^2$. By otherwise comparable experimental conditions, the solvent exchange method yielded SSMs of $R_M = 5.7\ k\Omega\ cm^2$.

Temperature. The influence of the temperature on the electrical properties of supported bilayers was investigated for various bilayer systems. In Figure 10, the measured membrane conductivities $g = R_M^{-1}$ are plotted versus the temperature T. Data of several experiments with bilayers of pure DOTAP as well as mixtures of 1:1 DOTAP/cholesterol and 4:6 DMTAP/cholesterol on ITO electrodes are shown. The variation of g by more than an order of magnitude for temperature changes of about 20 K demonstrates the strong dependence on the temperature. The change in the conductivity was reversible, and both heating and cooling cycles are shown.

Ion Concentration. Another environmental variable that is important for the electrical properties of supported bilayers is

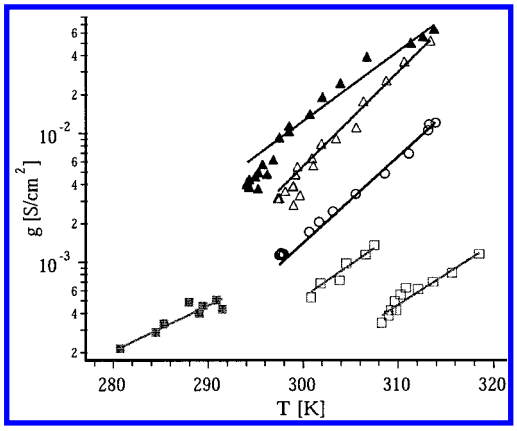

Figure 10. Semilogarithmic plot of the bilayer conductivity g versus T for pure DOTAP bilayers (▲, △) and mixed bilayers of 1:1 DOTAP/cholesterol (■, □) and 4:6 DMTAP/cholesterol (○) measured on ITO electrodes in 10 mM Hepes buffer (pH 7.5). The fitted lines represent the proportionality $g \propto e^T$ as suggested by Nagle and Scott's permeation model.

the ionic concentration of the electrolyte. A series of measurements with varying concentration of NaCl dissolved in 10 mM Hepes buffer at pH 7.5 was performed. The measured conductivities g of pure DOTAP bilayers and mixed bilayers of 1:1 (m/m) DOTAP/cholesterol and 4:6 (m/m) DMTAP/cholesterol on ITO substrates are plotted in Figure 11a. The conductivity increases with increasing ion content of the electrolyte and the dependence of g on the ionic concentration c is linear in first approximation. The lines connecting the data points in the order of measurement indicate the reversibility of the effect on g.

Figure 11b provides a plot of the membrane capacities C_M corresponding to the membrane conductivities in Figure 11a. Two effects become apparent from the sequence of the measurements indicated by lines between the data points. First, C_M tends to increase with increasing ion concentration. Second, the alterations are not reversible or at least not over the time frame of the experiments, which is on the order of a few hours.

Discussion

The experimental results suggest the correlation of the electrical response of SSMs to (I) the membrane−substrate interactions and to (II) the structural properties of the bilayer formed. Both play an important role regarding the kinetics of SSM formation and the properties of an equilibrated SSM system.

Membrane−Substrate Interactions. The dependence of R_M on the solution pH, the concentration of charged lipids in the membrane, and the bias potential indicates the dominating contribution of the electrostatic forces to the membrane−substrate interactions. In the case of a fluid-supported membrane that is not covalently bound or tethered to the surface (Figure 1), the forces interacting between the membrane and the solid substrate are the electrostatic force[23] f_{el} and the van der Waals force[24] f_{VdW} as well as the repulsive contributions due to hydration[24] f_{hyd} and membrane undulation[25] f_{steric}. These forces are defined as

$$f_{el}(d) = \frac{1}{\epsilon\epsilon_0} \cdot \frac{{\sigma_{s,s}}^2 + {\sigma_{s,m}}^2 + \sigma_{s,s}\sigma_{s,m}(e^{\kappa_D d} + e^{-\kappa_D d})}{(e^{\kappa_D d} - e^{-\kappa_D d})^2}$$

$$\text{with } \kappa_D = \sqrt{\frac{c{e_0}^2}{\epsilon\epsilon_0 kT}} \quad (10)$$

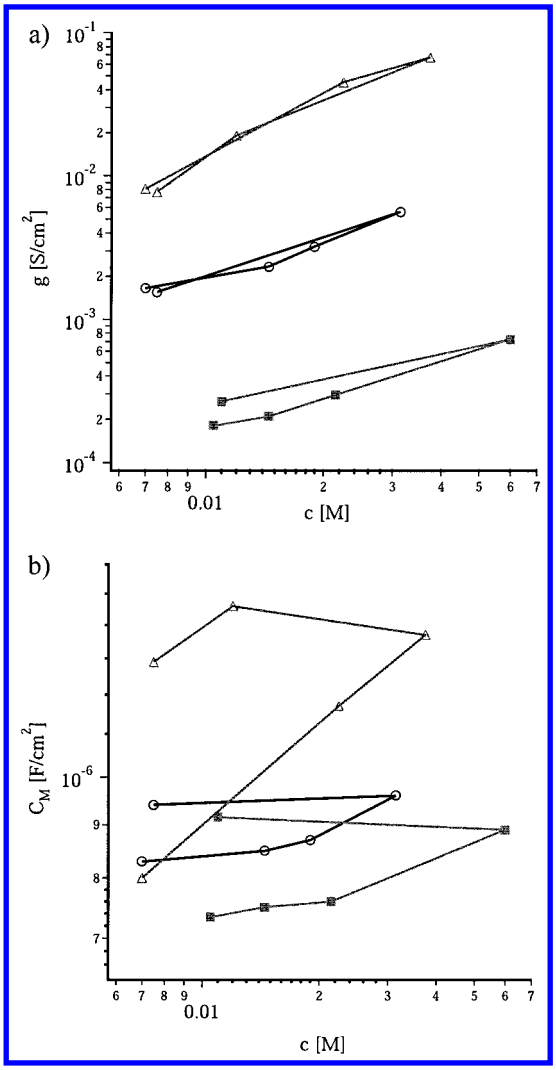

Figure 11. (a) Plot of the bilayer conductivity g as a function of the ion concentration c in the buffer solution (10 mM Hepes, pH 7.5). Data for pure DOTAP bilayers (△) and mixed bilayers of 1:1 DOTAP/cholesterol (■) and 4:6 DMTAP/cholesterol (○) are shown. The lines connecting the data points indicate the succession of the measurements. The first and the last data points of each experiment are at comparable conductivity values, demonstrating the reversibility of the observed variations. (b) Corresponding plot of the bilayer capacities C_M versus c. In contrast to the conductivity, the capacity variations monitored are not reversible within the experimental time frame.

$\sigma_{s,m}$ and $\sigma_{s,s}$ are the homogeneous surface charge densities of

$$f_{VdW}(d) = -\frac{A_H}{6\pi}\left(\frac{1}{d^3} - \frac{1}{(d + d_M)^3}\right) \quad (11)$$

$$f_{hyd} = f_0 \exp\left[-\frac{d}{\lambda_{hyd}}\right] \quad (12)$$

$$f_{steric} \approx \frac{(kT)^2}{2K_c d^3} \quad (13)$$

the adjacent planes of the membrane and substrate, respectively, surfaces separated by a neutral layer of salt solution, κ_D^{-1} is the Debye screening length, and d is the separation distance. A_H is the Hamaker constant, d_M is the thickness of the bilayer, λ_{hyd} is the hydration decay length, and K_c is the bending modulus of the membrane. The short-range repulsive part of the van der Waals force is neglected, since its value is very low for the

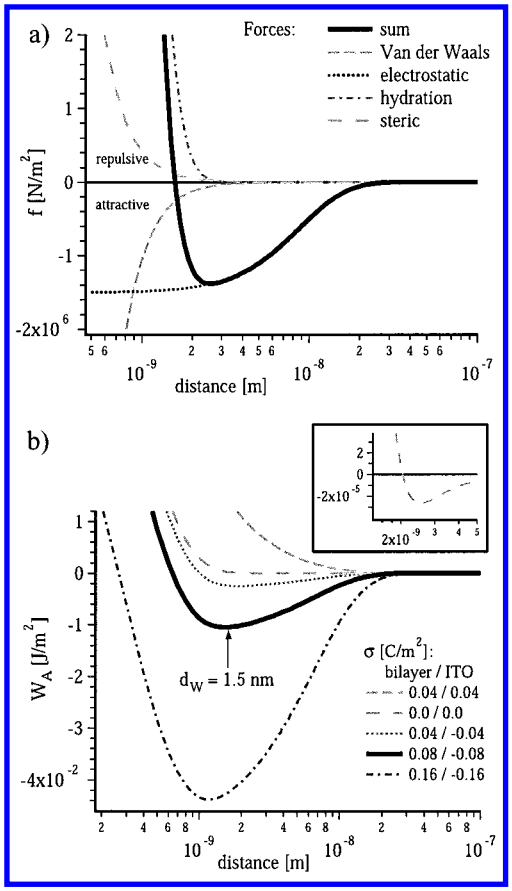

Figure 12. (a) Plot of the membrane−substrate forces and their sum as a function of the separation distance d. Variables used in the calculation: $A_H = 2.0 \cdot 10^{-20}$ J, $d_M = 4$ nm, $c^* = 10$ mM, $T = 300$ K, $\sigma_{SC} = -0.08$ C/m^2, $\sigma_M = 0.08$ C/m^2, $\epsilon = 80$, $\lambda_{hyd} = 0.26$ nm, $f_0 = 7.0 \cdot 10^8$ N/m^2, $K_c = 5$ kT. (b) Plot of the interaction potential as a function of d for different symmetric surface charge densities. The potential represented by the thick line was calculated from the sum of the forces in part a. The insert shows the curve of the potential of the neutral system around its minimum with ~1000-fold smaller scale.

distances considered here. In Figure 12a, a simulation of the interacting membrane−substrate forces is shown for a SSM scenario comparable to a 1:1 DOTAP/cholesterol membrane on ITO (parameters given in the caption). It is apparent that the sum of the forces is dominated by the long-range electrostatic attraction and the short-range hydration repulsion.

The adhesion of lipid bilayers to the surface of solid substrates is a consequence of the minimization of the surface free energy of the substrate by the bilayer adsorption. The forces interacting between the membrane and the substrate contribute to the adhesion energy according to

$$W_A(d) = \int_d^\infty [f_{VdW}(z) + f_{el}(z) + f_{hyd}(z) + f_{steric}(z)]\, dz \quad (14)$$

where z is the distance from the solid surface in normal direction. In Figure 12b, the potential resulting from the sum of the forces in Figure 12a is shown. In addition, potentials obtained for different symmetric surface charge densities are shown in order to visualize the contribution of the electrostatic interaction. Only in the case of very low surface charge ($<10^{-3}$ C/m^2) on both the membrane and the solid surface are the van der Waals forces comparable to the electrostatic interactions. The value of $W_A(d_W)$ at the minimum of the potential for zero net charge (see insert in Figure 12b) is about a factor of 1000 smaller in comparison to that for ± 0.16 C/m^2 (one charge per square nanometer). Within the range of buffer salt concentrations

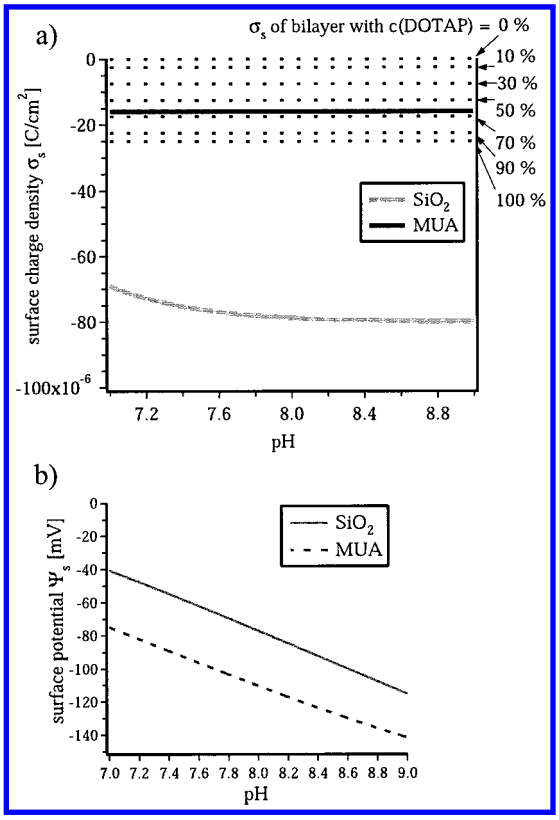

Figure 13. (a) Simulation of the surface charge density of Si/SiO$_2$ and Au/MUA substrates as a function of the solution pH. The dashed lines indicate the surface charge density of the different oppositely charged DOTAP/DOPC bilayers probed on these surfaces. The numbers at the left show the DOTAP concentration of the bilayer. (b) Simulation of the surface potentials corresponding to the surface charge densities of the solid substrates in part a.

generally used for SSM experiments (1−100 mM), the adhesion energy varies by about an order of magnitude, but f_{el} remains the dominating long-range contribution.

The importance of a significant amount of charged lipids to form electrically dense SSMs is in agreement with literature.[26,6] However, the maxima of R_M for DOTAP/DOPC membranes were yielded with a small fraction of charged lipid (Figure 7), which provides evidence that the membrane−substrate interactions are not the only decisive factor. In Figure 13a, a simulation of the surface charge densities[24] $\sigma_{s,s}$ of the Si/SiO$_2$ surface and the Au/MUA surface as a function of the solution pH is shown. The dashed lines indicate the surface charge densities of the different oppositely charged DOTAP/DOPC membranes probed on these surfaces. By consideration of the SSMs with maximal R_M values (10% DOTAP on Si/SiO$_2$; 30% DOTAP on Au/MUA), $\sigma_{s,s}$ of the substrate surfaces exceeds $\sigma_{s,m}$ of the membranes. The adhesion energy according to eqs 10−14 is maximal at 100% DOTAP on Si/SiO$_2$ and at 65% on Au/MUA. Two effects can account for the lower concentration of charged lipid in the SSMs with the best insulating properties. The first one is the electrostatic repulsion between the SSM and adjacent vesicles and lipid molecules within them, respectively. It increases the energy barrier that needs to be overcome for the fusion of further vesicles with or the incorporation of lipid molecules into the SSM. The second is the electrostatic repulsion between each of the individual charged lipid molecules within the SSM. Although the electrostatic contribution to the lateral pressure in the membrane is considered to be minor,[16] variations of the packing density of charged and uncharged lipid molecules

in a SSM of just a few percent may alter substantially the permeability of water and ions across the membrane.

The surface potentials[24] of the Si/SiO_2 and the Au/MUA surface as a function of the solution pH (Figure 13b) were calculated from the surface charge densities, σ_s, shown in Figure 13a. The more negative surface potential at higher pH increases the adhesion energy for oppositely charged SSMs and leads to increasing values of R_M, as seen in Figure 6a. This is in agreement with the observations of the SSM formation at different bias voltages (Figure 9). Interesting is the finding that the SSM formation can be reversed and an already-established membrane can be destabilized by lowering the pH (Figure 6b). Details of such an unbinding process of SSMs are so far unknown.

Structural Properties of SSMs. Cholesterol alters the physical properties of a lipid bilayer such as its thermodynamic behavior and mechanoelastic response.[27] The reduction of the ion permeability of unbound lipid bilayers by the addition of cholesterol was reported,[16,28] which is in agreement with the systematic increase of R_M with the concentration of cholesterol in the SSMs (Figure 8). To explain this effect, we employ Nagle and Scott's theory,[14] which correlates the bilayer permeability with structural details of the lipid bilayer. This theory was introduced as a model for the anomalous increase in the ionic permeability of phospholipid vesicles at the phase transition[28] and is preferable to molecular theories,[14−16,29,30] because the physics of the entire ensemble are considered. The transport of ions through the bilayer was attributed to the ion diffusion in the hydrocarbon region after entrapment. However, the diffusive movement is not the permeation-limiting process, but the ion entrapment is. The picture for the latter is that lateral density fluctuations open short-lived cavities in the headgroup region of the bilayers into which ions can enter. When the cavities close, the ions on the hydrocarbon side are trapped. The density fluctuations depend on the lateral compressibility of the bilayer. In the case of large fluctuations, small membrane-spanning pores instead of cavities in the headgroup regions may result. The formation of pores enables the transfer of ions together with their hydration shells. Whether ions enter cavities or are transferred through a pore depends on the energetic costs for the partial removal of the hydration shell, which in turn depends on the size of the cavities or pores formed. According to Nagle and Scott's model, the permeability coefficient is related to spontaneous area fluctuations by the series expansion

$$P_{M,j} = P_{0,j} + C_{1,j}\Delta a + C_{2,j}(\Delta a)^2 = P_{0,j} + C_{1,j}\Delta a + C'_{2,j}\kappa_T \quad (15)$$

where $P_{0,j}$ is the permeability of the jth ion species in the homogeneous state of the bilayer with uniform area a and $\Delta a = 0$. Permanent changes in the area alter the permeability proportional to Δa and $C_{1,j}$, whereas fluctuations $(\Delta a)^2$ cause an increase of the permeability proportional to $C_{2,j}$, provided that $C_{2,j}$ is positive. The area fluctuations $(\Delta a)^2$ are related to the lateral compressibility κ_T by $(\Delta a)^2 = -kT\cdot a\cdot\kappa_T$. Cholesterol lowers the compressibility κ_T and, hence, increases the electrical resistance of lipid bilayers. In addition, $(\Delta a)^2$ is proportional to the bilayer area a and, respectively, the area per lipid molecule times the number of molecules. Therefore, the density of lipids in a SSM that can be obtained for a specific combination of substrate material, bilayer composition, and deposition method determines the permeability of the SSM. Due to the required deposition process and the implicit energy barriers for the lipid incorporation during SSM formation and healing, the lipid density of a SSM will be lower than that of an unbound aggregate. The often orders-of-magnitude lower electrical resistance values of SSM in comparison to black lipid membranes or membrane patches from vesicles or cells are the direct consequence.

This model can also be employed to explain the temperature dependence observed for different SSMs (Figure 10). The series expansion of the permeability coefficient in eq 15, limited to the second order, can be transformed into

$$P_{M,j} = P_{0,j}\left[1 + \frac{C_{1,j}}{P_{0,j}}\Delta a + \frac{C_{2,j}}{P_{0,j}}(\Delta a)^2\right] = P_{0,j}\cdot e^{\xi\cdot\Delta a} \quad (16)$$

under the assumption that $C_{1,j}/P_{0,j} = (C_{2,j}/2P_{0,j})^{0.5} = \xi$. The thermal expansion coefficient α_T is defined as $\alpha_T = 1/a\cdot(da/dT)_\pi$, and the area variation Δa can be expressed by $\Delta a = (da/dT)_\pi\cdot\Delta T = a\cdot\alpha_T\cdot\Delta T$. The temperature variation can be transformed into $\Delta T = T - T_0$. By substituting Δa in eq 16 and considering that the T_0 term provides only a constant prefactor, the permeability coefficient exhibits the proportionality

$$P_{M,j} \propto e^{\xi a\alpha_T\cdot T} \quad (17)$$

This result is in agreement with the measured dependence of the conductivity g of supported bilayers as a function of the temperature (Figure 10). Fitting of the data according to this model yielded permeability coefficients of $P_M = 1\cdot10^{-9}$ m/s for the 1:1 DOTAP/cholesterol bilayer, $P_M = 7\cdot10^{-9}$ m/s for the 4:6 DMTAP/cholesterol bilayer, and $P_M = 5\cdot10^{-8}$ m/s for the pure DOTAP bilayer in 10 mM Hepes buffer (pH 7.5). An average value of $(\xi a\alpha_T) = 0.12 \pm 0.05$ K^{-1} was obtained. The product ξa is the corresponding exponential coefficient for relative area changes $\Delta a/a$. With $\alpha_T = 0.01$ K^{-1},[27] it follows $\xi a = 12$. According to these values, an increase in the area of the supported bilayer of ~6% would double its permeability, provided that the number of lipid molecules in the bilayer remains constant.

Ionic permeation across lipid bilayers is driven by transmembrane gradients such as electrostatic potential or osmotic pressure. The permeability coefficient P_M quantifies the ion transport through the membrane. Under the assumption of symmetric conditions at both membrane−electrolyte interfaces of the bilayer, the area normalized membrane conductivity g can be expressed by

$$g = \sum_j g_j = \sum_j \frac{i_j}{U_{AC}} \quad (18)$$

where U_{AC} is the amplitude of the voltage signal of the impedance analyzer. The net current density i_j of the j^{th} ion species across the bilayer can be derived as[16]

$$i_j = z_j F\cdot P_{M,j}\cdot\frac{\Delta c_j}{K_j}\left[1 - \exp\left(-\frac{e_0\Delta\Psi}{kT}\right)\right] \quad (19)$$

with the partition coefficient $K_j = \exp(-G_{0,j}/kT)$ and the potential difference $\Delta\Psi$ across the bilayer. The difference Δc_j between the ion concentrations at the respective interfaces $c_{int} = c^*\exp(-z_j e_0\Psi_{int}/kT)$ follows as

$$\Delta c_j = c^*\left[\exp\left(-\frac{z_j e_0\Psi_1}{kT}\right) - \exp\left(-\frac{z_j e_0\Psi_2}{kT}\right)\right] \quad (20)$$

where c^* denotes the bulk ion concentration of the electrolyte. By means of eqs 18−20, the approximately linear dependence

of the bilayer conductivity g on the ion concentration c (Figure 11a) can be explained.

The lower membrane resistance of SSMs prepared by solvent exchange instead of vesicle fusion may result from the differences in the formation processes. An optimized protocol for the mixing of the aqueous buffer with the 2-propanol solution may yield SSMs with improved insulating properties.

The observed systematic variation of the area-normalized membrane resistance values with the size of the electrode can be explained in terms of boundary effects that might occur at the border of the electrode. Two main effects occur at the electrode border. The first effect is the inhomogeneous potential distribution of the voltage signal applied to the electrode. According to Newman,[31] the current density derived from the potential distribution at the border of an electrode embedded into an insulating material, which is comparable to the situation of a thin-film electrode, is significantly higher than in the center of the electrode. This can cause a reduced electrical resistance for a membrane on such an electrode and lead to a dependence of the area-normalized R_M values on the ratio of the area to the circumference of the electrode. The second effect is a discontinuity in the membrane−substrate interactions and the resulting adhesion energy. The equilibrium separation distance between the membrane and the substrate might be different on the surface of the active electrode in comparison to the surface of the surrounding insulator. In addition, the transition region from one material to the other might expose a surface that is not well suited for lipid bilayer deposition and therefore perturbs the integrity of the SSM. Due to the finite electrical resistance of the ultrathin water layer between the membrane and the substrate, an electrically dense SSM has to cover not just the active electrode area and the border region but has to expand significantly onto the insulating substrate. Otherwise ionic current around the outer rim of a membrane patch can short-circuit the transmembrane conduction path.

Conclusion

Impedance spectroscopy is a powerful tool for the electrical characterization of SSMs. The experiments presented provide the basis for an in-depth analysis of the electrical properties of supported lipid bilayer membranes. By considering the submolecular structure of SSMs, a novel approach for an equivalent circuit model was derived exhibiting improved agreement between the model and the data. The improved agreement enables a more accurate determination of the membrane resistance R_M and the membrane capacity C_M. The observed dependence of the electrical properties of SSMs on compositional, preparational, and environmental parameters was explained in terms of membrane−substrate interactions and permeation models for lipid bilayer membranes. Electrostatic interactions between the lipid bilayer and the surface of the supporting substrate as well as the membrane compressibility were identified as key parameters for the formation of electrically dense SSMs. The enhanced understanding may facilitate the rational design of advanced biophysical applications utilizing SSMs for ion channel and membrane protein analysis.

Acknowledgment. The part of the work conducted at the TU Munich was funded by the Sonderforschungsbereich SFB 266, the Deutsche Forschungsgemeinschaft, and the Fond der chemischen Industrie.

References and Notes

(1) Sackmann, E. *Science* **1996**, *271*, 43−48.
(2) Cornell, B. A.; Braach-Maksvytis; King, L. G.; Osman, P. D. J.; Raguse, B.; Wieczorek, L.; Pace, R. J. *Nature* **1997**, *387*, 580−583.
(3) Michalke, A.; Schürholz, T.; Galla, H.-J.; Steinem, C. *Langmuir* **2001**, *17*, 2251−2257.
(4) Steinem, C.; Janshoff, A.; Sieber, M. *Bioelectrochem. Bioenerg.* **1997**, *42*, 213.
(5) Raguse, B.; Braach-Maksvytis; Cornell, B. A.; King, L. G.; Osman, P. D. J.; Pace, R. J.; Wieczorek, L. *Langmuir* **1998**, *14*, 648−659.
(6) Gritsch, S.; Nollert, P.; Jähnig, F.; Sackmann, E. *Langmuir* **1998**, *14*, 3118−3125.
(7) Kühner, M., Tampé, R., Sackmann, E. *Biophys. J.* **1994**, *67*, 217−226.
(8) Lindholm-Sethson, B. *Langmuir* **1996**, *12*, 3305−3314.
(9) Wong, J. Y.; Majewski, J.; Seitz, M.; Park, C. K.; Israelachvili, J. N.; Smith, G. S. *Biophysic. J.* **1999**, *77*, 1445−1457.
(10) Müller, P.; Rudin, D. O. *Nature* **1968**, *217*, 713−719.
(11) Sakmann, B.; Neher, E. *Single-Channel Recording*; Plenum Press: New York, 1985.
(12) Hillebrandt, H.; Wiegand, G.; Tanaka, M.; Sackmann, E. *Langmuir* **1999**, *15*, 8451−8459.
(13) Macdonald, J. R. *Impedance Spectroscopy*; John Wiley & Sons: New York, 1987.
(14) Nagle, J. F.; Scott, H. L. *Biochim. Biophys. Acta* **1978**, *513*, 236−243.
(15) Träuble, H. *J. Membrane Biol.* **1971**, *4*, 193−208.
(16) Cevc, G. *Biochim. Biophys. Acta* **1990**, *1031*, 311−382.
(17) Nardi, J.; Bruinsma, R.; Sackmann, E. *Phys. Rev. E* **1998**, *58*, 6340−6354.
(18) Aranda-Espinoza, H.; Chen, Y.; Dan, N.; Lubensky, T. C.; Nelson, P.; Ramos, L.; Weitz, D. A. *Science* **1999**, *285*, 394−397.
(19) Cole, K. S.; Cole, R. H. *J. Chem. Phys.* **1941**, *9*, 341−351.
(20) Fouss, R. M.; Kirkwood, J. G. *J. Am. Chem. Soc.* **1941**, *63*, 385−394.
(21) Reichl, L. E. *A Modern Course in Statistical Physics*, 2nd ed.; John Wiley & Sons: New York, 1998.
(22) Scher, H.; Shlesinger, M. F.; Bendler, J. T. *Physics Today* **1991**, 26−34.
(23) Parsegian, V. A.; Gingell, D. *Biophys. J.* **1972**, *12*, 1192−1204.
(24) Israelachvili, J. N. *Intermolecular and Surface Forces*; Academic Press: London, 1991.
(25) Helfrich, W.; Servuss, R.-M. *Il Nuovo Cimento* **1984**, *3 D*, 137.
(26) Steinem, C.; Janshoff, A.; Ulrich, W.-P.; Sieber, M.; Galla, H.-J. *Biochim. Biophys. Acta* **1996**, *1279*, 169−180.
(27) Sackmann, E. Physical Basis of Self-Organization and Function of Membranes: Physics of Vesicles. In *Structure and Dynamics of Membranes: From Cells to Vesicles*, 1st ed.; Lipowsky, R., Sackmann, E., Eds.; Elsevier Science B. V.: Amsterdam, 1995; Vol. 1, pp 213−304.
(28) Papahadjopoulos, K.; Jacobson, K.; Nir, S.; Isac, T. *Biochim. Biophys. Acta* **1973**, *311*, 330−348.
(29) Doniach, S. *J. Chem. Phys.* **1978**, *68*, 4912−4916.
(30) Parsegian, A. *Nature* **1969**, *221*, 84−846.
(31) Newman, J. *J. Electrochem. Soc.* **1966**, *113*, 501−502.